第 43 卷 第 13 期/2023 年 7 月/光学学报 研究论文

光学学报

双色激光场作用下水的高次谐波光谱移动

赵旭琳[1,2]，白丽华[1**]，白亚[2,3*]，刘鹏[2,3]

[1]上海大学物理系，上海 200444；

[2]中国科学院上海光学精密机械研究所强场激光物理国家重点实验室，上海 201800；

[3]中国科学院大学材料科学与光电工程中心，北京 100049

摘要 通过求解长度规范下的半导体布洛赫方程，分析了液态水在双色场驱动下发射高次谐波光谱的特征。研究表明，通过调节双色场中基频和倍频脉冲的相对相位，高次谐波光谱呈现出周期性调制的特征。在一个调制周期内，奇次谐波会随着相对相位的增加发生红移，而产率先增大后减小。时域分析结果表明，光谱移动源于正负半周期之间发射高次谐波频谱的干涉效应。

关键词 物理光学；高次谐波；双色激光场；光谱红移；频谱干涉

中图分类号 O437 **文献标志码** A **DOI**：10.3788/AOS222167

1 引 言

高次谐波是在强场激光脉冲与原子、分子、团簇、液体、固体的相互作用过程中产生的一种非微扰的高阶光学非线性效应[1-3]，是强场物理科学研究领域的前沿热点之一。高次谐波的应用广泛，如利用高次谐波来合成超短阿秒脉冲[4]、解码分子中的核动力学[5]、产生相干X射线[6]、重构固体能带[7]等。

近年来，液体作为新兴的高次谐波介质引起了科研人员的极大研究兴趣，和其他高次谐波介质相比，液体具有较高的电子密度，能承受更强的激光场，在提高高次谐波产率和产生更高强度高次谐波方面有很大的潜力。在原子分子的高次谐波上，Corkum等[3,8]提出的半经典“三步模型”很好地解释了高次谐波的产生过程，并成功地解释了高次谐波的发射效率和截止频率规则。在固体高次谐波上，半导体布洛赫方程（SBE）受到广泛认可，其物理机制主要涵盖了带间极化和带内电流两种动力学过程[9-14]。但是在液体的高次谐波上，尚未建立起一个成熟的实验和理论体系来探究液体内部的超快动力学机制。

目前，关于液体高次谐波的理论计算研究还处在探索阶段。Zeng等[15]构建了一条一维线性链来模拟液态水，采用统计学方法结合物理原理，模拟了强激光脉冲驱动下液态水的高次谐波产生过程，探讨了液体内电子的超快动力学规律。随后，Xia等[16]利用基于统计二能级共振的量子理论，在速度规范下求解含时薛定谔方程，揭示了液体中局域电荷共振态的作用。Neufeld等[17]通过构建水分子团簇，并且结合含时密度泛函理论，研究了液体的化学性质对高次谐波光谱的影响。

实验方面，Luu等[18]使用平面喷射技术制作出厚度约为1.9 μm的流体水薄膜，将激光脉冲作用到该水膜上，可观测到光子能量高达20 eV的高次谐波。理论上，考虑到水中电子的局域态特性，Luu等[18]将水看作宽带隙半导体，并近似计算出水的能带结构。通过求解SBE的方法对水的高次谐波进行模拟，借助多体相互作用和多价带参与的载流子动力学过程，很好地再现了实验观测现象。

由基频光和倍频光叠加而成的双色场[19-20]具有很强的不对称性，并且可以通过调整基频光和倍频光之间的时间延迟和相对强度进行调节。已有研究[21]表明，附加倍频光可以改变电子在激光场中的动力学过程，即“三步”模型中的“第二步”，引起不同电子路径之间的干涉。

本文讨论了双色激光场对高次谐波光谱频移的调制现象。通过求解长度规范下的SBE分析液态水在双色场驱动下发射高次谐波的特征，发现调节基频光和倍频光之间的相对相位差，可以调控高次谐波频谱中奇级次谐波的频率和产率，实现高次谐波谱的精细调节。利用小波变换法在时域中分离出正负半周期的谐波电流，探讨高次谐波的动力学机制，发现奇次谐波随双色场相对相位的红移和产率变化的原因主要为激

收稿日期：2022-12-22；**修回日期**：2023-02-28；**录用日期**：2023-03-06；**网络首发日期**：2023-03-13

基金项目：国家自然科学基金（11874373，12174412）、中国科学院科研仪器设备研制项目（YJKYYQ20180023）

通信作者：*pipbear@siom.ac.cn；** lhbai@163.com

光场中极性相反的正负半光周期产生谐波之间的频谱干涉。

2　计算方法

SBE从多电子体系的含时薛定谔方程出发，使用产生和湮灭算符来处理能带中电子-空穴对的产生和复合，使用Hartree-Fock近似来处理电子之间的库仑相互作用，进而将含时薛定谔方程转化成一组可解的偏微分方程[22-24]。长度规范下的二能带SBE[22]可写为

$$\mathrm{i}\hbar\frac{\partial}{\partial t}p_k=\left(\varepsilon_k^e+\varepsilon_k^h-\mathrm{i}\frac{\hbar}{T_2}\right)p_k-\left(1-n_k^e-n_k^h\right)\boldsymbol{d}_k\boldsymbol{E}(t)+\mathrm{i}e\boldsymbol{E}(t)\cdot\nabla_k p_k,\tag{1}$$

$$\hbar\frac{\partial}{\partial t}n_k^{e(h)}=-2\mathrm{Im}\left[\boldsymbol{d}_k\boldsymbol{E}(t)p_k^*\right]+e\boldsymbol{E}(t)\cdot\nabla_k n_k^{e(h)},\tag{2}$$

式中：p_k表示价带和导带之间的极化；$\varepsilon_k^{e(h)}$表示导带或价带的能量；T_2为退相时间，描述库仑相互作用导致载流子的失谐现象；$n_k^{e(h)}$表示载流子的动态演化；$\boldsymbol{d}_k$为随晶体动量变化的跃迁偶极矩；$\boldsymbol{E}(t)$为外加激光电场；e为电荷量；$\hbar$为约化普朗克常数；t为时间；$\boldsymbol{k}$为动量。

式(1)等号右侧的第一项表示体系随时间演化产生的相位积累，以及电子间散射引起的失相；第二项表示电子在能带间的跃迁，其中$\boldsymbol{d}_k\boldsymbol{E}(t)$表示带间极化；第三项表示电子或空穴在电场的驱动下在各自能带中的运动，其中$\boldsymbol{E}(t)\cdot\nabla_k$表示带内激发。此外，第三项会导致一个随时间变化的动量$\boldsymbol{k}$，其正比于电场强度：

$$\frac{\mathrm{d}}{\mathrm{d}t}\boldsymbol{k}(t)=-\frac{e}{\hbar}\boldsymbol{E}(t)。\tag{3}$$

载流子的贡献分为带间和带内电流两个部分：

$$\boldsymbol{J}_{\mathrm{inter}}(t)=\sum_k\left[\boldsymbol{d}_k p_k+\mathrm{c.c}\right],\tag{4}$$

$$\boldsymbol{J}_{\mathrm{intra}}(t)=\sum_{e(h),k}e\upsilon_k^{e(h)}n_k^{e(h)}(t),\tag{5}$$

式中：$\upsilon_k^{e(h)}=\frac{1}{\hbar}\frac{\partial\varepsilon_k^{e(h)}}{\partial\boldsymbol{k}}$，为群速度。因此，高次谐波光谱的计算公式为

$$S_{\mathrm{HHG}}\propto\left|\omega^2\boldsymbol{J}_{\mathrm{inter}}(\omega)+\mathrm{i}\omega\boldsymbol{J}_{\mathrm{intra}}(\omega)\right|^2,\tag{6}$$

式中：ω为频率。

3　分析与讨论

所使用的双色激光场为

$$E(t)=f(t)\left[E_0\cos(\omega_0 t)+aE_0\cos(2\omega_0 t+\phi)\right],\tag{7}$$

式中：$f(t)=\exp\left\{-2\ln\left[2\left(\frac{t}{\tau}\right)^2\right]\right\}$为高斯型包络；$E_0$和$\omega_0$分别为基频光场的光电场强度和频率；$a$为倍频相对基频的场强比值；$\phi$为基频光和倍频光的相对相位差；$\tau$为激光脉冲的半峰全宽；$E(t)$为双色激光场的大小。驱动激光波形如图1(a)所示，其中T为基频脉冲光周期，基频脉冲的波长$\lambda=1500\ \mathrm{nm}$，半峰全宽$\tau=30\ \mathrm{fs}$，光电场强度$E_0=5\times10^{11}\ \mathrm{W/cm^2}$。

利用上述双色激光场结合SBE，所用能带从文献[18]得出，拟合得到的能带如图1(b)所示，其中$2\pi\cdot a^{-1}$为第一布里渊区宽度；所用的跃迁偶极矩是通过kp理论($d_{\mathrm{cv}}(k)=\frac{\mathrm{i}d_0\left[\varepsilon_{\mathrm{c}}(0)-\varepsilon_{\mathrm{v}}(0)\right]}{\left[\varepsilon_{\mathrm{c}}(k)-\varepsilon_{\mathrm{v}}(k)\right]}$，其中$\varepsilon_{\mathrm{c}}(0)$为$k=0$时的导带能量，$\varepsilon_{\mathrm{v}}(0)$为$k=0$时的价带能量，$\varepsilon_c(k)$为导带，$\varepsilon_{\mathrm{v}}(k)$为价带，$d_0=3.0\ \mathrm{a.u.}$)计算得到的。需要说明的是，本研究只考虑跃迁偶极矩的模，忽略了跃迁偶极矩的相位。

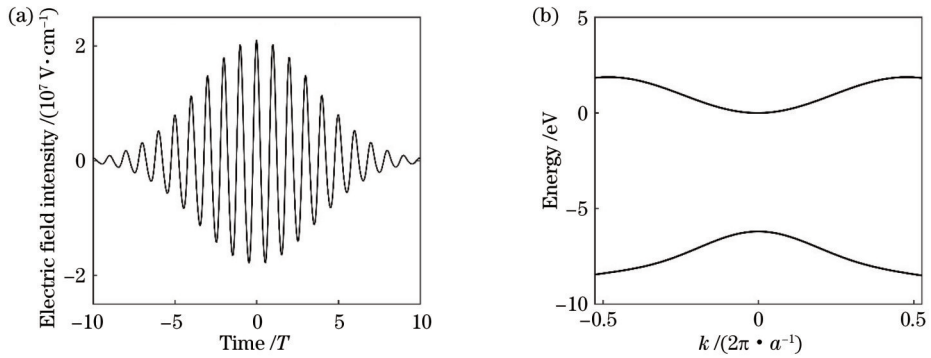

图1　入射激光电场和能带结构。(a)相对相位$\phi=0.2\pi$的入射激光电场；(b)计算所用的能带结构

Fig. 1　Electric field intensity of driving pulse and the band structure. (a) Electric field intensity of driving pulse at relative phase of $\phi=0.2\pi$; (b) band structure used in the calculation

水产生高次谐波光谱的典型结果如图2所示，由于倍频电场的引入打破了激光电场的对称性，因此谐波光谱中包含偶次谐波。高次谐波的产率随着级次的增大先迅速下降，随后保持稳定，形成“平台区”，最终在23级次附近截止。此外，高次谐波光谱中还有一个显著特征，即谐波中心频率相对于$N\omega_0$(其中N为谐波阶数)所定义的谐波频率发生了蓝移。

根据激光电场的非绝热效应[25-26]：在激光脉冲的

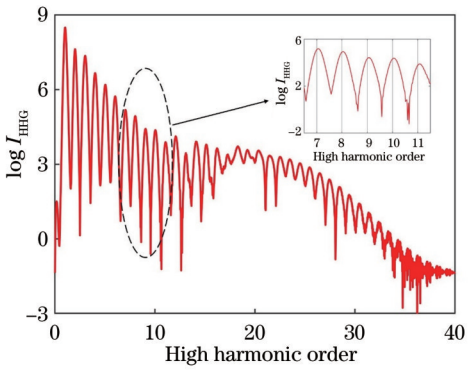

图 2 双色场相对相位 $\phi=0.2\pi$ 时水产生的高次谐波光谱

Fig. 2 High-order harmonic spectra from liquid water at the relative phase of $\phi=0.2\pi$

上升沿，每一个激光周期的激光电场峰值振幅大于前一个激光周期，导带中电子的加速时间延长，再碰撞时辐射光子能量附加一个增加量，从而导致高次谐波光谱蓝移；在激光脉冲的下降沿，每一个激光周期的激光电场峰值振幅小于前一个激光周期，高次谐波光谱红移。最终高次谐波光谱的净频移取决于激光脉冲的上升沿和下降沿的相对贡献[25-26]。因此，谐波光谱的频移取决于其发射时间是在激光脉冲的上升沿还是下降沿。为了解释观测到的高次谐波光谱蓝移现象，对高次谐波发射的时频谱进行分析，结果如图 3 所示。显然，高次谐波发射主要发生在激光脉冲的上升沿，这正是高次谐波光谱蓝移的原因。

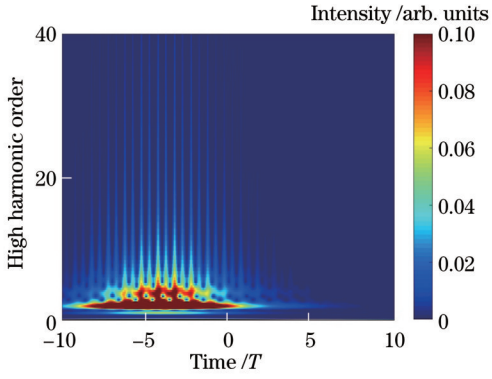

图 3 双色场相对相位 $\phi=0.2\pi$ 时的高次谐波电流的时频分析谱图，时间零点为电场包络峰值

Fig. 3 Time-frequency analysis spectra of the calculated high harmonic current at the relative phase of $\phi=0.2\pi$, and time zero is the peak value of the electric field envelope

由于高次谐波光谱取决于脉冲电场振荡，通过引入延时精密可调谐的倍频激光场对基频光场进行调制，有助于进一步对光周期内高次谐波产生过程进行观测。高次谐波光谱随双色场相对相位的变化如图 4 所示。可以明显看到，奇级次谐波的强度和中心频率都随相对相位呈周期性变化。在一个基频调制周期内（对应双色场相位为 0～π），随着相对相位差的增大，谐波中心频率不断红移，谐波产率则先增大后减小。这种频移现象也普遍存在于其他频率比的双色场驱动的情形中，比如采用基频和三倍频（$\omega_0+3\omega_0$），也能观测到类似的频谱调制现象。

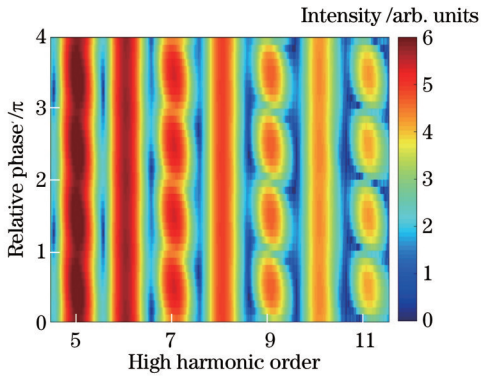

图 4 不同相对相位时的双色场高次谐波光谱

Fig. 4 High-order harmonic spectra changed with relative phase

由于正负半光周期产生的谐波具有不同的时频特征，需要分开讨论正负半光周期的贡献，以及它们之间的频谱干涉。使用时间滤波窗口将正负半光周期的谐波电流分离，再分别变换到频率域，得到半周期分辨的谐波频谱，如图 5 所示。从图 5 所示的不同相位差正负半周期的谐波频谱可以看出：当相位差从 0 增加到 0.5π 时，正半周期对于奇级次高次谐波的贡献基本不变且大于负半光周期的贡献，负半周期对于奇级次高次谐波的贡献增加；当相位差从 0.6π 增加到 0.9π 时，正半周期对于奇级次高次谐波的贡献减小，负半周期对于奇级次高次谐波的贡献基本不变且大于正半周期的贡献。

图 6 所示为不同相位差的 H9、H11 的半周期分辨的谐波频谱移动。从图 6 可以看出，在负半周期产生的谐波是先蓝移后红移，而在正半周期产生的谐波始终红移。

下面将进一步解释正负半周期之间的频谱干涉过程。两个相干信号的相位差由初始相位差和产生的时间差决定[27]，即

$$J(s,\phi)=J_{\mathrm{p}}(s,\phi)-J_{\mathrm{n}}(s,\phi)\exp\left[\mathrm{i}s\omega_0\Delta t_{\mathrm{r}}(\phi)\right], \quad (8)$$

式中：$J(s,\phi)$ 为第 s 级次的谐波电流；$J_{\mathrm{p}}(s,\phi)$ 为正半周期产生的谐波电流；$J_{\mathrm{n}}(s,\phi)$ 为负半周期产生的谐波电流；$\Delta t_{\mathrm{r}}(\phi)$ 为不同相对相位差正负半周期的复合时间差；$s\omega_0\Delta t_{\mathrm{r}}(\phi)$ 表示由半周期时间差导致的相位变化；等号右边的负号表示在相邻半周期之间，外加光强方向相反。

根据 SBE 模型，电子在 t_1 时刻从价带跃迁到导带，在价带留下空穴，在激光场的作用下，电子以 $v_{\mathrm{e}}=\nabla\varepsilon_k^{\mathrm{e}}\left[k(t)\right]$ 的速度运动，空穴以 $v_{\mathrm{h}}=\nabla\varepsilon_k^{\mathrm{h}}\left[k(t)\right]$ 的速度运动，电子和空穴的运动方向相反，经过一段时间后，

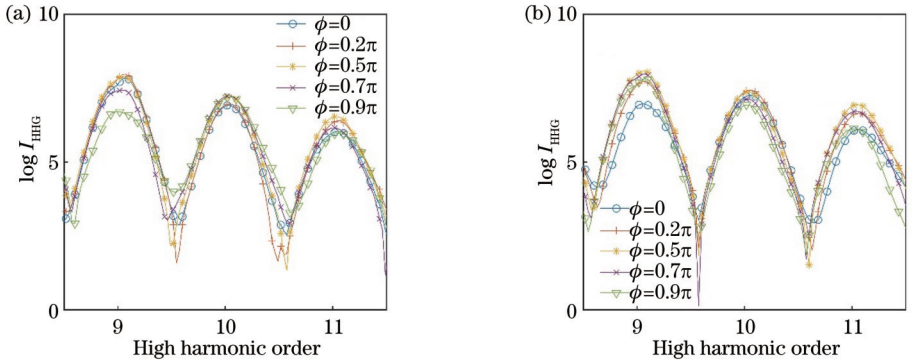

图 5　正负半周期分别贡献的谐波频谱。(a)正半周期;(b)负半周期。

Fig. 5　Contributions to harmonic spectra from positive half-cycle and negative half-cycle. (a) Positive half-cycle; (b) negative half-cycle

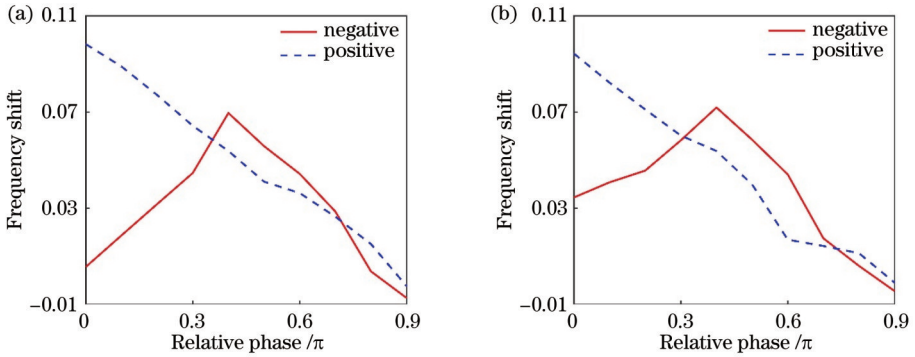

图 6　H9、H11的正负半周期分别贡献的谐波频移。(a) H9;(b) H11

Fig. 6　Frequency shift of H9 and H11 from positive half-cycle and negative half-cycle. (a) H9; (b) H11

电子在实空间内的位移为 $x_e=\int_{t_1}^{t_r}\nabla\varepsilon_k^e\left[k(t)\right]\mathrm{d}t$，空穴在实空间内的位移为 $x_h=\int_{t_1}^{t_r}\nabla\varepsilon_k^h\left[k(t)\right]\mathrm{d}t$。当 $x_e=x_h$ 时，电子和空穴复合产生一个高能光子：$\hbar\omega_{HHG}=\varepsilon_k^e\left[k(t_r)\right]-\varepsilon_k^h\left[k(t_r)\right]$，其中 t_r 为复合时刻。

分别计算了不同相位差下正负半光周期H9的复合时间，并给出了复合时间差 $\Delta t_r(\phi)$，如表1所示（T_0 为计算所在的光周期）。从表1可以看出，当相位差从0增加到0.9π时，在负半周期复合的电子发射的谐波先蓝移后红移，而在正半周期复合的电子发射的谐波始终红移，这个规律和图6所示结果一致。根据表1，复合时间差 $\Delta t_r(\phi)$ 先减小后增大，再结合前文对于图5的分析和式(8)，可以推断出：奇级次谐波随着相位差的增大不断红移，且产率先增大后减小。综上可知，在一个调制周期内，计算得到的奇级次谐波随着相位差增大不断红移是正负半光周期之间频谱干涉的结果。

表1　不同 ϕ 下正负半光周期H9的复合时间

Table 1　Recombination time of H9 with positive and negative half-cycles at different ϕ

ϕ	t_r in negative half-cycle / T_0	High harmonic order in negative half-cycle	t_r in positive half-cycle / T_0	High harmonic order in positive half-cycle	$\Delta t_r(\phi)/T_0$
0	0.8189	9.1730	0.1383	9.5136	0.6806
0.1π	0.8113	9.2706	0.1410	9.5142	0.6703
0.2π	0.8050	9.3445	0.1406	9.4871	0.6644
0.3π	0.8010	9.3876	0.1379	9.4454	0.6631
0.4π	0.7987	9.3994	0.1329	9.3902	0.6658
0.5π	0.7996	9.3711	0.1257	9.3198	0.6739
0.6π	0.8023	9.3090	0.1176	9.2429	0.6847
0.7π	0.8073	9.2128	0.1087	9.1557	0.6986
0.8π	0.8140	9.0907	0.1001	9.0692	0.7139
0.9π	0.8216	8.9590	0.0929	8.9923	0.7287

4 结 论

通过求解长度规范下的SBE,研究了液态水在双色场驱动下发射高次谐波的时频特征,分析了谐波光谱随电场波形调制发生频率移动的规律。研究结果表明:在一个调制周期内,计算中得到的奇级次谐波随着相位差增大不断红移是正负半光周期之间频谱干涉的结果;在单色驱动激光脉冲中引入延时精密可调且具有不同频率的微扰激光脉冲,可以改变电子在激光场中的动力学过程,从而实现高次谐波光谱的调谐。

参 考 文 献

[1] McPherson A, Gibson G, Jara H, et al. Studies of multiphoton production of vacuum-ultraviolet radiation in the rare gases[J]. Journal of the Optical Society of America B, 1987, 4(4): 595-601.

[2] Ferray M, L'Huillier A, Li X F, et al. Multiple-harmonic conversion of 1064 nm radiation in rare gases[J]. Journal of Physics B, 1988, 21(3): L31-L35.

[3] Corkum P B. Plasma perspective on strong field multiphoton ionization[J]. Physical Review Letters, 1993, 71(13): 1994-1997.

[4] Paul P M, Toma E S, Breger P, et al. Observation of a train of attosecond pulses from high harmonic generation[J]. Science, 2001, 292(5522): 1689-1692.

[5] Baker S, Robinson J S, Haworth C A, et al. Probing proton dynamics in molecules on an attosecond time scale[J]. Science, 2006, 312(5772): 424-427.

[6] Popmintchev T, Chen M C, Popmintchev D, et al. Bright coherent ultrahigh harmonics in the keV X-ray regime from mid-infrared femtosecond lasers[J]. Science, 2012, 336(6086): 1287-1291.

[7] Vampa G, Hammond T J, Thiré N, et al. All-optical reconstruction of crystal band structure[J]. Physical Review Letters, 2015, 115(19): 193603.

[8] Lewenstein M, Balcou P, Ivanov M Y, et al. Theory of high-harmonic generation by low-frequency laser fields[J]. Physical Review A, 1994, 49(3): 2117-2132.

[9] Higuchi T, Stockman M I, Hommelhoff P. Strong-field perspective on high-harmonic radiation from bulk solids[J]. Physical Review Letters, 2014, 113(21): 213901.

[10] Ghimire S, DiChiara A D, Sistrunk E, et al. Observation of high-order harmonic generation in a bulk crystal[J]. Nature Physics, 2011, 7(2): 138-141.

[11] Vampa G, McDonald C R, Orlando G, et al. Theoretical analysis of high-harmonic generation in solids[J]. Physical Review Letters, 2014, 113(7): 073901.

[12] Schubert O, Hohenleutner M, Langer F, et al. Sub-cycle control of terahertz high-harmonic generation by dynamical Bloch oscillations[J]. Nature Photonics, 2014, 8(2): 119-123.

[13] Li J B, Zhang X, Fu S L, et al. Phase invariance of the semiconductor Bloch equations[J]. Physical Review A, 2019, 100(4): 043404.

[14] Jiang S C, Chen J G, Wei H, et al. Role of the transition dipole amplitude and phase on the generation of odd and even high-order harmonics in crystals[J]. Physical Review Letters, 2018, 120(25): 253201.

[15] Zeng A W, Bian X B. Impact of statistical fluctuations on high harmonic generation in liquids[J]. Physical Review Letters, 2020, 124(20): 203901.

[16] Xia C L, Li Z L, Liu J Q, et al. Role of charge-resonance states in liquid high-order harmonic generation[J]. Physical Review A, 2022, 105(1): 013115.

[17] Neufeld O, Nourbakhsh Z, Tancogne-Dejean N, et al. *Ab initio* cluster approach for high harmonic generation in liquids[J]. Journal of Chemical Theory and Computation, 2022, 18(7): 4117-4126.

[18] Luu T T, Yin Z, Jain A, et al. Extreme-ultraviolet high-harmonic generation in liquids[J]. Nature Communications, 2018, 9(1): 3723.

[19] Yang W F, Lin Y C, Chen X Y, et al. Wave mixing and high-harmonic generation enhancement by a two-color field driven dielectric metasurface[J]. Chinese Optics Letters, 2021, 19(12): 123202.

[20] Tan J, Xu S L, Han X, et al. Resolving and weighing the quantum orbits in strong-field tunneling ionization[J]. Advanced Photonics, 2021, 3(3): 035001.

[21] Madhusudhan P, Das R, Bhardwaj P, et al. Strong-field ionization of N_2 and CO molecules using two-color laser field[J]. Journal of Physics B, 2022, 55(23): 234001.

[22] Golde D, Meier T, Koch S W. High harmonics generated in semiconductor nanostructures by the coupled dynamics of optical inter- and intraband excitations[J]. Physical Review B, 2008, 77(7): 075330.

[23] Luu T T, Wörner H J. High-order harmonic generation in solids: a unifying approach[J]. Physical Review B, 2016, 94(11): 115164.

[24] Cao J Y, Li N, Bai Y, et al. Even-order high-harmonic generation from solids in velocity gauge[J]. Chinese Optics Letters, 2021, 19(4): 043201.

[25] Li G C, Zheng Y H, Ge X C, et al. Frequency modulation of high-order harmonic generation in an orthogonally polarized two-color laser field[J]. Optics Express, 2016, 24(16): 18685-18694.

[26] Du H C, Xue S, Wang H Q, et al. Nonadiabatic spectral redshift of high-order harmonics with the help of a VUV pulse [J]. Physical Review A, 2015, 91(6): 063844.

[27] Cao J Y, Li F S, Bai Y, et al. Inter-half-cycle spectral interference in high-order harmonic generation from monolayer MoS_2[J]. Optics Express, 2021, 29(4): 4830-4841.

High-Harmonic Spectral Shift of Water Under Two-Color Laser Fields

Zhao Xulin[1,2], Bai Lihua[1**], Bai Ya[2,3*], Liu Peng[2,3]

[1]*Department of Physics, Shanghai University, Shanghai* 200444, *China*;

[2]*State Key Laboratory of High Field Laser Physics, Shanghai Institute of Optics and Fine Mechanics, Chinese Academy of Sciences, Shanghai* 201800, *China*;

[3]*Center of Materials Science and Optoelectronics Engineering, University of Chinese Academy of Sciences, Beijing* 100049, *China*

Abstract

Objective High harmonic is a crucial technology for generating bright and coherent light sources in extreme ultraviolet (EUV) and X-rays for a wide range of applications, including material science, chemistry, and biology. High harmonic is also used in attosecond science, which studies the ultrafast dynamics of electrons in atoms and molecules on their natural timescale of attoseconds (10^{-18} s). High harmonic has traditionally been studied in gases and solids, but recent research has shown that it can also be observed in liquids. High harmonic in liquids offers several advantages over traditional gas-phase and solid-phase high harmonic. Firstly, liquids have higher electron densities than gases. Second, liquids can withstand higher laser intensities and can repair damage automatically compare with solids. Thus, high harmonic in liquids is a promising candidate for a compact and brighter EUV source. Therefore, it is crucial to reveal the underlying mechanism of liquid-phase high harmonic. However, there are many fundamental questions in liquid-phase high harmonic. In theory, Zeng *et al*. conducted a study in 2020 to investigate liquid-phase high harmonic by using a disordered linear chain and proposed a formula that could quantify the cutoff energy. Subsequently, Xia *et al*. proposed a statistical two-level model and revealed the role of localized charge-resonance states in high harmonic from disordered liquids. In experiments, Luu *et al*. reported the observation and detailed characterization of high harmonic in the EUV region from liquid water. Here, we study the high harmonic from liquid water by solving the semiconductor Bloch equations (SBE) in length gauge and investigate the modulation of the spectral shift in harmonic spectra driven by two-color laser fields. Our findings indicate that manipulating the relative phase of two-color laser fields can control the frequency and yield of odd harmonics and allow for the fine tuning of the high harmonic spectrum. We believe that our primary findings will be helpful for future studies on strong-field and attosecond electron dynamics in liquids.

Methods First, by solving the SBE in length gauge, the high harmonic from water driven by two-color laser fields consisting of a fundamental field and its second harmonic is studied. Then, time-frequency analysis of the calculated high-order harmonic current is carried out by wavelet transform to gain more information about the high harmonic process. After that, the contributions from positive and negative half-cycles in the time domain are artificially separated and respectively transformed into the frequency domain to see how the inter-half-cycle interference affects the frequency shift of different harmonic orders. Next, the frequency shift of H9 and H10 from positive and negative half-cycles in different phase differences is calculated. Furthermore, the time of re-encounter in the positive and negative half-cycles dictated by the motion of electrons and holes in real space is calculated.

Results and Discussions A typical high harmonic spectrum (Fig. 2) of water shows that the harmonic spectrum contains both odd and even harmonics. The generation of even harmonics is the consequence of the asymmetric two-color field. A clear sign of a plateau is shown, followed by a cutoff at the 23rd harmonic. Another important feature of the spectrum is that the harmonics are all blue-shifted. It can be attributed to the nonadiabatic effect. The time-frequency analysis (Fig. 3) shows that the high-order harmonics are mainly generated in the rising edge of the fundamental pulse. In the rising edge of the laser field, the high harmonic possesses a positive chirp and thus leads to a blue-shifted spectrum. Furthermore, it is shown that by changing the relative phase of two-color laser fields, the even- and odd-harmonics are periodically modulated (Fig. 4). As the relative phase is tuned from 0 to π, the redshift of odd-harmonics increases, and the odd-harmonics yield increases first and then decreases. As the relative phase is tuned from 0 to 0.5π(0.6π-0.9π), the contribution of the positive half-cycle to odd-order high harmonic is greater (less) than that of the negative half-cycle (Fig. 5). As the relative phase is tuned from 0 to π, high harmonic produced in the negative half-cycle is blue-shifted first and then red-shifted, while high harmonic produced in the positive half-cycle is always red-shifted (Fig. 6). According to the different contributions from different half-cycles (Fig. 5) and the phase difference results from the time interval between two adjacent half-cycles (Table 1), the interference between the positive and negative half-cycles (Eq. 8) is analyzed. In conclusion, these phenomena can be attributed to inter-half-cycle interference between positive and negative half-cycles.

Conclusions In this study, high harmonic in liquid water driven by two-color laser fields consisting of a fundamental field and its second harmonic is investigated. Our analysis focuses on the spectral blueshift, and time-frequency analysis reveals that the high harmonics are mainly generated during the rising edge of the fundamental pulse, resulting in a blue-shifted harmonic spectrum. Besides, by tuning the relative phase of two-color laser fields, both the amplitude and the center frequency of high harmonic can be modulated. These phenomena can be attributed to the interference of high harmonic emitted from positive and negative half-cycles. This study might shed new light on the attosecond electron dynamics in liquids and the tuning of liquid-phase high harmonic.

Key words physical optics; high-harmonic; two-color laser field; spectral redshift; spectral interference